J. Paduano

L. Valavani

A. H. Epstein

Gas Turbine Laboratory,
Department of Aeronautics and Astronautics,
Massachusetts Institute of Technology,
Cambridge, MA 02139

Parameter Identification of Compressor Dynamics During Closed-Loop Operation

A low-speed axial research compressor has been fitted with movable inlet guide vanes to allow for feedback stabilization of rotating stall. A model exists whose structure captures the input-output behavior, and stabilization of rotating stall is possible using this model. Quantitative identification of the parameters in the rotating stall model requires the ability to identify MIMO dynamics, which may be unstable, during closed loop operation. The 'instrumental variable' technique is presented as the basic approach to this problem. The necessary extensions to the basic technique are discussed, and the resulting algorithm is applied. Experimental results are presented which verify that the methodology yields useful estimates.

1 Introduction

Rotating stall is a fluid mechanical phenomenon which besets axial compressors at low flow conditions. It is characterized by a severely nonaxisymmetric distribution of axial velocity around the annulus of the compressor, taking the form of a wave or "stall cell," which propagates in the circumferential direction at a fraction of the rotor speed. Because the nonuniformity travels with respect to both the rotor and stator vanes, both are subject to large amplitude unsteady velocities and thus loading which can cause vibration, fatigue, and severe heating. Additionally, rotating stall in jet engines reduces the thrust and often leads to surge, an even more severe and debilitating instability involving the entire compression system.

The transition from normal compressor operation into rotating stall is depicted on a typical compressor pressure rise-mass flow characteristic in Fig. 1. This plot relates the nondimensionalized flow rate—known as flow coefficient, ϕ—to the nondimensional pressure rise. The lowest flow rate at which the compressor can operate with axisymmetric flow is point A, the peak of the characteristic. At lower flow coefficients, an abrupt transition occurs into rotating stall (point B). This condition will persist until the flow is increased to point C. Thus, there exists a severe "hysteresis," that is, range of flow coefficients at which two stable operating conditions exist—one of which is undesirable and often unsafe.

Traditionally, stall has been avoided by avoiding operation near point A. This solution necessitates leaving an ample "stall margin," so that transients in flow rate and ingestion of nonaxisymmetric or otherwise disturbing flow will not drive the system to the rotating stall operating condition. A concomitant performance penalty is paid, because the highest pressure rise and, sometimes, the highest efficiency lie at a flow coefficient below the minimum imposed by the stall margin requirement. It is therefore of interest to reduce the minimum allowable flow coefficient, without putting the system in danger of stall and/or surge.

This is the motivation for a number of recent papers, which describe the phenomenology (Kerrebrock, 1977; Greitzer, 1976; and Greitzer, 1980), fluid mechanics (Moore, 1984; Hynes and Greitzer, 1987; and Epstein et al., 1989) and active control (Epstein et al., 1989; Paduano et al., 1991; and Paduano, 1992), of rotating stall. In this paper, we will take the results of these papers as a starting point, giving only a brief description of the active control results and the model presented in (Paduano et al., 1991 and Paduano, 1992). We will then present techniques for identification of the model parameters.

1.1 Active Control of Rotating Stall. Consider the schematic diagram of an axial compressor in Fig. 2. It consists of an upstream annular duct, a set of inlet guide vanes (IGVs), a compressor, a downstream annular duct, and a throttle. Normally, flow through the compressor is circumferentially

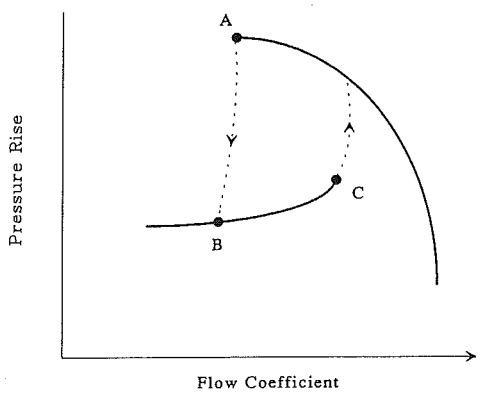

Fig. 1 Typical pressure rise characteristics for an axial compressor

Contributed by the Dynamics Systems and Control Division for publication in the JOURNAL OF DYNAMIC SYSTEMS, MEASUREMENT, AND CONTROL. Manuscript received by the DSCD November 20, 1991; revised manuscript received January 5, 1993. Associate Technical Editor: J. L. Stein.

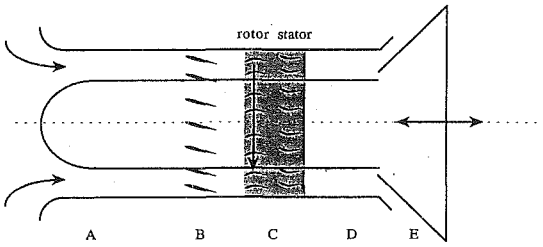

Fig. 2 Schematic of the active control research compressor. A-inlet duct, B-IGVs, C-compressor, D-exit duct, E-throttle

uniform (axisymmetric), and a single non-dimensional measure of fluid velocity determines the system state. This measure is the flow coefficient, which is axially velocity normalized by rotor speed at the mean radius:

$$\phi = \frac{\text{(axial velocity)}}{\text{(rotor speed)}}. \tag{1}$$

Under certain conditions, however, the flow through the compressor can become non-axisymmetric, that is, circumferential "waves" of perturbation flow coefficient, $\delta\phi$, can exist. In this case, the system can be completely characterized by two terms: the annulus averaged flow coefficient, $\bar{\phi}$, and the circumferential perturbation on this average at some axial station:

$$\phi = \bar{\phi} + \delta\phi(\theta, t), \tag{2}$$

where θ is circumferential position and t is time. Velocity waves $\delta\phi$ will tend to propagate around the annulus in the direction of rotor rotation. The time evolution of these waves determines the stability of the system. If they damp out with time, the system is stable and will return to axisymmetric operation. If they grow, the system is unstable and the waves will continue to grow until nonlinear effects take over—this condition is known as rotating stall, and usually consists of one or more stall cells rotating around the annulus at a fraction of the rotor speed.

Recently (Paduano et al., 1991), active control was successfully applied to this problem in a low-speed single-stage research compressor. The experimental setup is shown in Fig. 3. Eight hot wire anemometers, arranged around the annulus near the compressor face, measure the velocity perturbations. A digital computer processes these signals and creates a feedback signal to a set of 12 movable inlet guide vanes (IGVs). The IGVs are individually mounted on digitally controlled high-bandwidth (80 Hz) servomotors. This allows independent control of the IGV incidences, $\delta\gamma_k$. For the wave shapes that are of interest in our experiment, these 12 blade deflections around the circumference can be considered as a continuous "actuation wave," $\delta\gamma(\theta,t)$. This actuation wave can be commanded in response to the measured wave of perturbation axial velocity, a feedback scheme which allows the compressor to operate axisymmetrically at values of $\bar{\phi}$ which would normally be unstable to flow perturbations $\delta\phi(\theta,t)$.

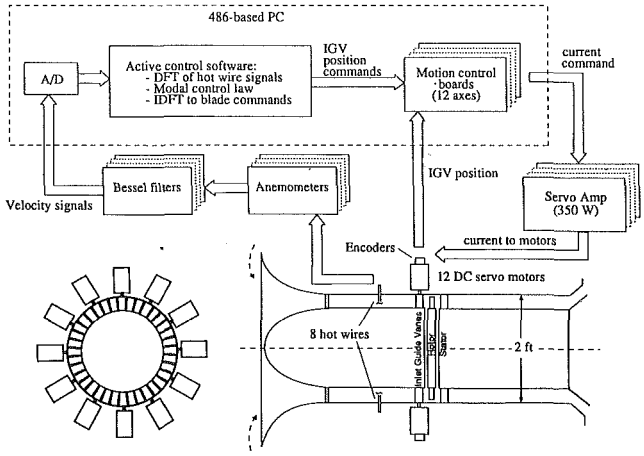

Fig. 3 Hardware components of the active control research compressor

Epstein et al. (1989) and Paduano (1992) present a model for the input-output dynamics of this system, which will be reviewed briefly in Section 1.2. Although the *structure* of this

Nomenclature

$B(z)$, $A(z)$ = numerator, denominator polynomials in discrete SISO model (13)

$B_n(z)$, $A_n(z)$ = numerator, denominator polynomials in discrete rotating stall model (11)

$A_u(z)$ = polynomial whose roots coincide with the unstable roots of $A(z)$ (32)

$A_s(z)$ = polynomial whose roots coincide with the stable roots of $A(z)$ (32)

a_i = denominator coefficients of z^{-1} in discrete models (11, 13)

b_i = numerator coefficients of z^{-1} in discrete models (11, 13)

b_{r_n}, b_{i_n}, g_{i_n} = control power parameters for continuous rotating stall model (8)

$C(z)$, $D(z)$ = numerator, denominator polynomials in discrete SISO noise model (21)

$E(z)$, $F(z)$ = polynomials in alternate representation of discrete noise model (33)

e = prediction error (15)

$G_n(s)$ = transfer function between $\tilde{\gamma}_n(s)$ and $\tilde{\phi}_n(s)$, (4)

$G_{r_n}(s)$ = transfer function between $u_{1_n}(s)$ and $y_{1_n}(s)$, (7)

$G_{i_n}(s)$ = transfer function between $u_{1_n}(s)$ and $y_{2_n}(s)$, (7)

$G_c(z)$ = dynamics in the feedback path of closed-loop system (Fig. 4)

$G_s(z)$ = dynamics of forward path of closed-loop system (Fig. 4)

k = time index for discrete systems

L = term to be minimized in the log-likelihood function (30)

n = spatial mode number

t = time, seconds

r = external input for discrete SISO closed-loop system (30, Fig. 4)

r_{1_n}, r_{2_n} = nth spatial cosine and sine coefficients of the external input (Fig. 4)

u = input of discrete SISO model (13)

u_{1_n}, u_{2_n} = nth spatial cosine and sine coefficients of $\delta\gamma$, (5)

y = output of discrete SISO model (13)

y_{1_n}, y_{2_n} = nth spatial cosine and sine coefficients of $\delta\phi$, (5)

p_i = poles of $A(z)$ whose magnitudes are ≥ 1 (32)

q, w = dummy signals used in derivation of closed-loop prediction (Section 2.4)

β = vector of instruments in AML method (29)

η = parameter vector in AML method (27)

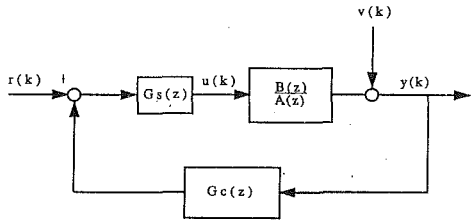

Fig. 4 Feedback loop layout and notation

model captures the experimentally observed behavior extraordinarily well, quantitative prediction of system dynamics is not as yet possible a priori. Instead, experimental searches and parameter identification techniques are used to aid in control system design. Parameter identification using spectral analysis techniques allows open-loop dynamics to be determined (Paduano, 1992), but such methods fail during closed-loop operation. In order to extend the operating range, it becomes necessary to identify the unstable dynamics: this identification must necessarily be done during closed-loop operation. Information about unstable compressor dynamics is also of interest from a experimental fluid mechanics point of view; such information has never before been measured.

This paper presents the results of applying an instrumental variable parameter identification procedure to the active control research compressor during closed-loop operation at various values of $\bar{\phi}$ (some of which are unstable). The instrumental variable (IV) technique (Ljung, 1987) was chosen for this study because of its flexibility. For instance, it can be adapted to MIMO or non-standard systems. Also, with proper filtering, the IV estimates can be made to approach the maximum likelihood estimates. Finally, with careful choice of instruments, the problems normally associated with IV identification during closed-loop stabilization can be alleviated. These issues will presented in Section 2, after a brief description of the system dynamics. In Section 3, experimental results will be shown for the active control research compressor.

1.2 Dynamic System Description. As described above, we assume that the system state can be completely characterized by $\bar{\phi}$ and the perturbation $\delta\phi(\theta,t)$ at some axial station. $\bar{\phi}$ can be fixed in an experimental environment by a throttle downstream of the compressor. This defines the system operating point, and "equilibrium" is defined as axisymmetric flow, i.e., $\delta\phi = 0$. We are interested in the dynamics of $\delta\phi(\theta,t)$ and the stability of the equilibrium point. We are also interested in the *forced* dynamics of this system, that is, the transfer characteristics between $\delta\gamma(\theta,t)$ and $\delta\phi(\theta,t)$.

Hynes and Greitzer (1987), Epstein et al. (1989), and Paduano (1992) all present a linearized fluid mechanical model for this distributed system. It can be shown that this model has a modal structure which allows the system to be "diagonalized" as follows: If we represent the functions $\delta\phi$ and $\delta\gamma$ in terms of their spatial Fourier series:

$$\delta\phi(\theta,t) = \sum_{n\neq 0} \tilde{\phi}_n(t) \cdot e^{jn\theta},$$

$$\delta\gamma(\theta,t) = \sum_{n\neq 0} \tilde{\gamma}_n(t) \cdot e^{jn\theta}, \tag{3}$$

then the transfer characteristics between $\tilde{\gamma}_n$ and $\tilde{\phi}_n$ are completely decoupled, i.e.,

$$\tilde{\phi}_n(s) = G_n(s) \cdot \tilde{\gamma}_n(s), \quad \text{for } n = \cdots -2, -1, 1, 2, \cdots. \tag{4}$$

This represents a tremendous simplification of the distributed dynamics and allows standard control techniques to be applied. Furthermore, the system dynamics are dominated by the lower modes; by feeding back only the first few modes ($|n| = 1, 2, 3$), substantial improvement in operating range can be achieved (Paduano et al., 1991).

The system diagonalization can also be represented in terms of Fourier sine and cosine coefficients, so that all terms in the equations are real. If we represent the input and output functions as

$$\delta\phi(\theta,t) = \sum_{n>0} y_{1_n}(t) \cdot \cos(n\theta) + \sum_{n>0} y_{2_n}(t) \cdot \sin(n\theta),$$

$$\delta\gamma(\theta,t) = \sum_{n>0} u_{1_n}(t) \cdot \cos(n\theta) + \sum_{n>0} u_{2_n}(t) \cdot \sin(n\theta), \tag{5}$$

Nomenclature (cont.)

$\tilde{\gamma}_n$ = nth spatial Fourier coefficient of $\delta\gamma$, (3)
δ = perturbation quantity
$\delta\gamma(\theta,t)$ = circumferential distribution of IGV deflection, degrees
ν = additive (colored) noise random process (13, 21)
$\delta\phi(\theta,t)$ = circumferentially nonuniform ϕ perturbation, (2)
ϕ = compressor axial flow coefficient, (1)
$\bar{\phi}$ = annulus averaged flow coefficient, (2)
$\tilde{\phi}_n$ = nth spatial Fourier coefficient of $\delta\phi$, (3)
Φ = regressors vector (system inputs and outputs) in IV prediction (14)
Φ_n = regressors matrix for rotating stall nth mode (36)
θ = circumferential position, radians
Θ = parameter vector in IV prediction equation (14)
σ_n = stability parameter for nth mode of continuous rotating stall model (8, 10)
ω_{rs_n} = rotation frequency for nth mode of continuous rotating stall model (8, 10)
ξ = white noise random process (21)
ζ = vector of instruments in IV method (16)
ζ_n = matrix of instruments for rotating stall nth mode (41)
φ = regressors vector in AML method (27)
$(\hat{\cdot})$ = prediction or estimation
$(\cdot)^f$ = filtered version of argument
$(\cdot)^T$ = transpose
$(\cdot)_n$ = nth mode version of the argument
$(\cdot)^c$ = alternate signal which is highly correlated with the argument
$(\cdot)_i$ = ith column of matrix argument, ith element of vector argument
$(\cdot)_{ij}$ = (i, j) element of matrix argument
$E\{\cdot\}$ = expected value
$Z\{\cdot\}$ = Z-transform
$Z^{-1}\{\cdot\}$ = inverse Z-transform
IGV = inlet guide vane
IV = instrumental variable
RIV = refined instrumental variable
AML = approximate maximum likelihood
NF = noise-free
TR = test-repeat
ML = maximum likelihood
ROC = region of convergence
ac = anticausal
snc = stable, noncausal
uc = unstable, causal
uac = unstable,, anticausal

then the transfer characteristics become

$$\begin{bmatrix} y_{1_n} \\ y_{2_n} \end{bmatrix} = [T_n(s)] \cdot \begin{bmatrix} u_{1_n} \\ u_{2_n} \end{bmatrix}, \quad \text{for } n = 1, 2, \cdots \tag{6}$$

where $T_n(s)$ is skew-symmetric because of the symmetry of the annulus:

$$[T_n(s)] = \begin{bmatrix} G_{r_n}(s) & -G_{i_n}(s) \\ G_{i_n}(s) & G_{r_n}(s) \end{bmatrix},$$

$$G_n(s) = G_{r_n}(s) + jG_{i_n}(s). \tag{7}$$

The structure of $G_n(s)$ is predicted by the fluid mechanical model, and is best expressed by giving the ODE for the system. Again, we can use either the complex Fourier coefficient representation or the real MIMO representation:

$$\dot{\tilde{\phi}}_n = (\sigma + j\omega_{rs})_n \cdot \tilde{\phi}_n + (b_r + jb_i)_n \cdot \tilde{\gamma}_n + jg_{i_n} \cdot \dot{\tilde{\gamma}}_n \tag{8}$$

or, using the identities $\phi_n = 1/2(y_{1_n} - j\,y_{2_n})$ and $\gamma_n = 1/2\,(u_{1_n} - j\,u_{2_n})$:

$$\begin{bmatrix} \dot{y}_{1_n} \\ \dot{y}_{2_n} \end{bmatrix} = \begin{bmatrix} \sigma & -\omega_{rs} \\ \omega_{rs} & \sigma \end{bmatrix}_n \begin{bmatrix} y_{1_n} \\ y_{2_n} \end{bmatrix} + \begin{bmatrix} b_r & -b_i \\ b_i & b_r \end{bmatrix}_n \begin{bmatrix} u_{1_n} \\ u_{2_n} \end{bmatrix} + \begin{bmatrix} 0 & -g_i \\ g_i & 0 \end{bmatrix}_n \begin{bmatrix} \dot{u}_{1_n} \\ \dot{u}_{2_n} \end{bmatrix}. \tag{9}$$

These two representations each have their advantages: The complex form is compact and contains no redundant parameters. It also automatically satisfies the symmetry conditions in the annulus. The real system, on the other hand, is standard from the point of view of control theory—it has no complex numbers, and the two-state nature of the system is clear ($\tilde{\phi}_n$ consists of a phase and a magnitude, so the system (8) isn't *strictly* SISO).

The physical significance of σ_n and ω_{rs_n} can be seen by substituting the homogeneous solution to (8) into (3), for some mode n:

$$\delta\phi(\theta,t) = e^{jn\theta} \cdot e^{(\sigma_n + j \cdot \omega_{rs_n})t} = e^{j(n\theta + \omega_{rs_n})t} \cdot e^{\sigma_n t} \tag{10}$$

The second equality shows that $\omega_{rs_n} \cdot t$ alters the phase of the wave, causing it to rotate; thus ω_{rs_n} is the 'rotating stall frequency' for the nth mode. It is also clear that $\sigma_n \cdot t$ alters the size of the rotating wave in (10); thus σ_n is the rotating stall stability parameter for the nth mode.

Techniques exist to convert these continuous state-space systems to discrete systems for the purpose of identification using digitally sampled data (Åström and Wittenmark, 1984). In this paper we will convert freely from continuous to discrete-time systems and back without emphasizing the details of such conversion. The discrete-time equivalent system for the above dynamics can be written as:

$$\begin{bmatrix} y_{1_n} \\ y_{2_n} \end{bmatrix} = \frac{B_n(z)}{A_n(z)} \cdot \begin{bmatrix} u_{1_n}(z) \\ u_{2_n}(z) \end{bmatrix} + \nu(z)$$

where

$$A_n(z) = (1 + a_1 z^{-1} + a_2 z^{-2})_n, \tag{11}$$

$$B_n(z) = \begin{bmatrix} (b_1 + b_2 z^{-1})(1 + z^{-1}) & -(b_3 + b_4 z^{-1} + b_5 z^{-2}) \\ (b_3 + b_4 z^{-1} + b_5 z^{-2}) & (b_1 + b_2 z^{-1})(1 + z^{-1}) \end{bmatrix}_n,$$

z is the Z-transform variable and n is the mode number. We have also added $\nu(k)$ to model disturbances. We will be concerned here with the identification of the parameter set

$$\Theta_n = [a_1\ a_2\ b_1\ b_2\ b_3\ b_4\ b_5]_n^T, \quad n = 1, 2, \cdots. \tag{12}$$

The discrete-time parameters Θ_n can subsequently be converted to the continuous domain, giving σ_{rs}, ω_{rs}, b_r, b_i, and g_i in (8) and (9). We would like to accomplish this identification task for unstable dynamics, during closed-loop stabilization. Section 2 describes our approach to this problem.

2 Instrumental Variable Method

The organization of this section is as follows: Section 2.1 reviews the basic IV method for SISO systems. Section 2.2 outlines Young's Refined IV-Approximate Maximum Likelihood (RIV-AML) method. Modifications to this approach necessary to handle the closed loop case are discussed in Section 2.3, and modifications for unstable plants are discussed in Section 2.4. Finally, a brief discussion of how the MIMO estimation for the rotating stall system is efficiently computed appears in Section 2.5.

2.1 Basic IV Procedure. Consider the system

$$y(z) = \frac{B(z)}{A(z)} \cdot u(z) + \nu(z) \tag{13}$$

where:

$$A(z) = (1 + a_1 z^{-1} + a_2 z^{-2} + \cdots),$$
$$B(z) = (b_1 + b_2 z^{-1} + b_3{}^{-2} + \cdots),$$

and $\nu(k)$ represents the (possibly colored) noise corrupting the measurements. We can build a one-step-ahead predictor for this system:

$$\hat{y}(k) = \Phi^T(k) \cdot \hat{\Theta}, \tag{14}$$

where:

$$\Phi(k) = [-y(k-1) - y(k-2) \cdots u(k)\ u(k-2)\ u(k-2) \cdots]^T,$$
$$\hat{\Theta} = [\hat{a}_1\ \hat{a}_2\ \cdots\ \hat{b}_1\ \hat{b}_2\ \hat{b}_3\ \cdots]^T$$

and the $\hat{}$ indicates prediction or estimation. The prediction error can then be written as

$$e(k) = y(k) - \Phi^T(k) \cdot \hat{\Theta}. \tag{15}$$

The instrumental variable (IV) method (Ljung, 1987) finds the value of $\hat{\Theta}$ which will cause the error to be uncorrelated with some chosen set of instruments

$$\zeta(k) = [\zeta_1(k)\ \zeta_2(k)\ \cdots]^T. \tag{16}$$

This condition can be written as follows:

$$\hat{\Theta} = \text{sol}\left\{\frac{1}{N}\sum_{k=1}^{N} \zeta(k) \cdot e(k) = 0\right\}, \tag{17}$$

where sol{•} indicates that $\hat{\Theta}$ is the value of Θ for which the equation in brackets is satisfied. Substituting in Eq. (15):

$$\hat{\Theta} = \text{sol}\left\{\frac{1}{N}\sum_{k=1}^{N} \zeta(k)\,(y(k) - \Phi^T(k) \cdot \hat{\Theta}) = 0\right\} \tag{18}$$

The philosophy of the IV approach is this: If the instruments are chosen to be related to the system inputs and outputs, and $\hat{\Theta}$ does *not* satisfy (17), then there is additional information about the input-output dynamics left in the prediction error. Therefore, a good estimate of Θ should extract this information, making the correlation in (17) disappear.

The solution to (18) is

$$\hat{\Theta} = \left[\frac{1}{N}\sum_{k=1}^{N} \zeta(k)\Phi^T(k)\right]^{-1} \cdot \left[\frac{1}{N}\sum_{k=1}^{N} \zeta(k)y(k)\right]. \tag{19}$$

The IV method will have good convergence and consistency properties if the following two conditions are met:

$$\sum_{k=1}^{N} \zeta(k)\Phi^T(k) \quad \text{nonsingular} \tag{20a}$$

$$E\left\{\sum_{k=1}^{N} \zeta(k)\nu(k)\right\} = 0 \tag{20b}$$

Condition (20a) guarantees invertibility in (19), and also indicates that ζ is correlated with the system dynamics, which is necessary for Eq. (17) to yield good estimats. In fact, if $\zeta(k)=\Phi(k)$, then (20a) is satisfied trivially and the estimate becomes the least-squares estimate of Θ.

Condition (20b) specifies that the instruments be uncorrelated with the noise, so that colored noise will not corrupt the estimates. This condition is often not met in the least-squares case ($\zeta(k)=\Phi(k)$), hence the need for a different set of instruments. Prefiltered versions of the elements of $\Phi(k)$ are usually used in this case. Ljung (1987) gives a complete description of the IV method, its convergence and consistency properties, and methods for constructing instruments which are uncorrelated with the noise.

2.2 Young's Refined Instrumental Variable—Approximate Maximum Likelihood (RIV-AML) Technique. Many filtering schemes have been proposed for constructing the instruments $\zeta(k)$ in the IV procedure. Young (1984) has developed a particularly attractive set of prefilters and instruments in the context of maximum likelihood estimation, for the following noise model:

$$v(z)=\frac{C(z)}{D(z)}\cdot\xi(z). \tag{21}$$

In this formulation, both $C(z)$ and $D(z)$ are monic, and $\xi(k)$ is an uncorrelated sequence with Gaussian amplitude distribution over the sample interval:

$$\underline{\xi}\sim N(0,\Sigma^2\cdot I)\quad \underline{\xi}=[\xi(1),\ \xi(2),\ \cdots,\ \xi(T)].$$

In Young's approach, the input-output data is first prefiltered, which introduces a new set of variables:

$$y^f(z)\equiv\frac{D}{A\cdot C}\cdot y(z);\quad u^f(z)\equiv\frac{D}{A\cdot C}\cdot u(z);$$

$$\hat{y}^f(z)\equiv\frac{B}{A}\cdot u^f(z) \tag{22}$$

Young shows that, with these definitions, the maximum-likelihood estimate can be stated as the solution of an IV problem:

$$\hat{\Theta}=\left[\frac{1}{N}\sum_{k=1}^{N}\zeta(k)\Phi_f^T(k)\right]^{-1}\cdot\left[\frac{1}{N}\sum_{k=1}^{N}\zeta(k)y^f(k)\right] \tag{23}$$

where

$$\zeta(k)=[-\hat{y}^f(k-1)\ -\hat{y}^f(k-2)\cdots\ u^f(k)\ u^f(k-1)\ u^f(k-2)\cdots]^T$$

and

$$\Phi_f(k)=[-y^f(k-1)\ -y^f(k-2)\cdots\ u^f(k)\ u^f(k-1)\ u^f(k-2)\cdots]^T,$$

In other words, if the above defined variables and instruments are used, then $\hat{\Theta}$ is the maximum likelihood estimate. This is called the refined IV, or RIV, estimate.

Of course, the polynomials $A(z)$, $B(z)$, $C(z)$, and $D(z)$ in Eq. (22) are not known a priori. Initial estimates of these must be made, and the RIV method applied iteratively to improve the estimates. The parameters in $\hat{\Theta}$ constitute the updates for $\hat{A}$ and $\hat{B}$ in such a scheme, so iteration on Θ is sufficient as a search on the maximum likelihood estimates of A and B. C and D, on the other hand, are not estimated by the procedure. Therefore, an estimation algorithm for C and D must be added to the iteration.

Young provides an approximate maximum likelihood approach to do exactly that. It provides a way to estimate C and D, based on the current estimates of A, B, C, and D. The basic philosophy is to form an error term based on the current estimates $\hat{A}$ and $\hat{B}$. This error term is then considered to be the output of a dynamic system driven by white noise, and the dynamics are estimated using a procedure similar to the RIV procedure described above. The specifics of this procedure, called approximate maximum likelihood (AML), are as follows:

We first take the prediction error $e(k)$ in (15) as a measurement of $v(k)$:

$$\begin{aligned} v(z)&=y(z)-\frac{B(z)}{A(z)}\cdot u(z)\\ \Rightarrow\hat{v}(z)&=y(z)-\hat{y}(z)\\ &=e(z).\end{aligned} \tag{24}$$

The dynamics in (21) are then written

$$D(z)\cdot\hat{v}(z)=C(z)\cdot\xi(z). \tag{25}$$

A "one-step-ahead predictor" for this system is

$$\hat{v}(k)=\varphi^T\hat{\eta} \tag{26}$$

where:

$$\begin{aligned}\varphi&=[-\hat{v}(k-1)\ -\hat{v}(k-2)\cdots\xi(k-1)\ \xi(k-2)\cdots]^T\\ \eta&=[d_1\ d_2\cdots c_1\ c_2\cdots]^T\end{aligned} \tag{27}$$

To compute an approximate maximum likelihood estimate of the noise system, prefilter as follows:

$$\begin{aligned}\hat{v}^f(k)&=\frac{1}{\hat{C}(z)}\cdot\hat{v}(k)\\ \hat{\xi}^f(k)&=\frac{1}{\hat{C}(z)}\cdot\hat{\xi}(k)=\frac{\hat{D}(z)}{\hat{C}(z)}\cdot\hat{v}^f(k)\end{aligned} \tag{28}$$

The estimate for the noise model is then:

$$\hat{\eta}=\left[\frac{1}{N}\sum_{k=1}^{N}\beta(k)\varphi^T(k)\right]^{-1}\cdot\left[\frac{1}{N}\sum_{k=1}^{N}\beta(k)\hat{v}(k)\right] \tag{29}$$

where:

$$\beta(k)=[-\hat{v}^f(k-1)\ -\hat{v}^f(k-2)\cdots\hat{\xi}^f(k-1)\ \hat{\xi}^f(k-2)\cdots]^T$$

The notation here has been made as similar to the IV notation as possible, to show the parallel between this procedure and the RIV procedure described above. Note that we used some set of past estimates $\hat{A}$, $\hat{B}$, $\hat{C}$, and $\hat{D}$ to allow us to best estimate $\hat{\eta}$, which is the updated estimate for C and D. Young gives more detail about the properties of the estimates, and also gives a recursive algorithm for its application.

We now have an estimation procedure for C and D, which can be integrated into the iteration for the maximum likelihood estimates of A and B. The complete RIV-AML recursion algorithm, then, is (Young, 1984)

1. Begining with initial estimates for $\hat{A}(z)$, $\hat{B}(z)$, $\hat{C}(z)$, and $\hat{D}(z)$.
2. Use the AML procedure (Eqs. (24)–(29)) to update $\hat{C}$ and $\hat{D}$.
3. Use the RIV procedure (Eqs. (22)–(23)) to update $\hat{A}$ and $\hat{B}$.
4. Go to 2, repeat with the new values of $\hat{A}$ and $\hat{B}$.

One purpose of the filters in Eqs. (22) is to eliminate as much as possible the effect of the colored noise on the outputs. Such "prewhitening" attempts to insure that $y^f(k)$ is uncorrelated with the disturbances $v(k)$. $y^f(k)$ must be uncorrelated with $v(k)$ in order to satisfy Eq. (20b), because $y^f(k)$ is a part of the instruments. The filtered inputs $u^f(k)$, which make up the remainder of the instruments, must also be uncorrelated with $v(k)$ in order to satisfy Eq. (20b). During open-loop operation, this condition is automatically satisfied, because $\xi(k)$ in Eq. (21) is uncorrelated with $u(k)$. During closed-loop operation, however, $v(k)$ and $u(k)$ *are correlated* (this will be shown in the next section). The above method must, therefore, be modified for closed-loop identification. This is the subject of the following section.

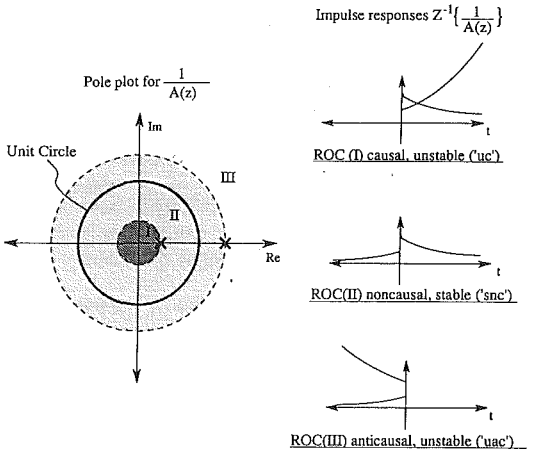

Fig. 5 Example of different impulse responses associated with the same transfer function. The inverse *Z*-transform of *A*(*z*) can be computed over any of the three regions of convergence (ROCs) shown (I, II, or III). The impulse response in each case is the sum of the truncated exponentials at right.

2.3 Choice of Closed-Loop Instruments. Figure 4 shows the layout and notation for closed-loop operation. The system dynamics remain as in Eq. (13). In addition, we introduce the external input signal, $r(k)$, and the following feedback law:

$$u(z) = G_s(z) \cdot [r(z) - G_c \cdot y(z)], \tag{30}$$

where $G_c(z)$ and $G_s(z)$ are rational transfer functions representing dynamics in the feedback and forward path. For the rotating stall controller, these dynamics are well defined, so here we will assume that they are known. Since $y(k)$ is corrupted by $v(k)$, $u(k)$ will now be correlated with the noise, and Eq. (20*b*) will be violated:

$$u(z) = G_s \cdot \left(r(z) - G_c \cdot \left(\frac{B}{A} \cdot u(z) + v(z) \right) \right),$$

$$\Rightarrow E\left\{ \sum_{k=1}^{N} \zeta(k) v(k) \right\} \neq 0,$$

because $\zeta(k)$ contains $u(k)$. This is a very real problem which does not constitute a mere theoretical technicality. In a high-gain feedback situation such as occurs during stabilization of unstable dynamics, it renders the IV methods described so far useless. Fortunately, these methods regain their applicability if the proper substitutions are made to insure that the instruments fulfill Eqs. (20).

Söderström et al. (1987) and Wang and Cao (1988) discuss in detail the problem of closed-loop estimation, and the methods they describe will be used here. The idea is to replace $\{y(k), u(k)\}$ in the computation of the instruments with some $\{y^c(k), u^c(k)\}$ which are highly correlated with their respective counterparts (condition (5.20*a*), but which are uncorrelated with the disturbances (condition (5.20*b*)). The two methods used to accomplish this are described below. In both cases, we assume $r(k)$ is a known external excitation.

Method I: Test-Repeat (TR) Instrumental Variable. This method, introduced by Wang and Cao (1988), achieves uncorrelated instruments by repeating the experiment twice, with identical $r(k)$ in both cases. The measured inputs and outputs for the two tests are denoted $\{u(k), y(k)\}$ and $\{u^c(k), y^c(k)\}$. The procedure is to use one of these input-output pairs to compute the instruments, and the other to compute the estimates. The RIV-AML estimation proceeds exactly as described in Section 2.2, using $\{u^c(k), y^c(k)\}$ to compute the instruments and $\{u(k), y(k)\}$ to compute the parameter estimates (the roles of the two input-output pairs can be switched).

Using identical $r(k)$ in the two tests insures high correlation between the instruments and the measurements, and poses no particular difficulty in a digital control environment. Also, because $v(k)$ and $v^c(k)$ are incurred at different times, they are uncorrelated, which means that the instruments (from the first test) will be uncorrelated with the disturbances (from the second test) even if the system is operating closed loop. Wang and Cao (1988) prove these claims, and discuss the consistency properties of the Test Repeat (TR) method.

Method II: Noise-Free (NF) Instruments. Both Wang and Cao (1988) and Söderström et al. (1987) discuss this method, which uses noise-free (NF) simulation of the test to generate the instruments. In this case $\{u^c(k), y^c(k)\}$ comes from a simulation, using an a priori estimate of the system dynamics (i.e., $\hat{\Theta}$). $v^c(k)$ will thus be identically zero. The same input $r(k)$ is then applied to the real system to get $\{u(k), y(k)\}$. The RIV-AML algorithm can now be applied, using $\{u^c(k), y^c(k)\}$ to compute the instruments and $\{u(k), y(k)\}$ as the measurements (in this case the roles of the two input-output pairs cannot be switched).

The same reasoning applies here as in the TR case. The noise-free instruments will naturally be uncorrelated with the noise from the experiment (condition (20*a*)). The degree of correlation between the instruments and the measurements (condition (20*b*)) will depend on the accuracy of the a priori estimate of the system dynamics, but (except in trivial cases) some correlation will exist. Closed-loop operation changes none of these observations. Söderström et al. (1987) and Wang and Cao (1988) discuss NF estimation more rigorously.

2.4 Modification of the RIV-AML Prefilters for Unstable Plant Dynamics. The test-repeat instrumental variable (TR/IV) and the noise-free instrumental variable (NF/IV) methods allow indentification of system dynamics during closed-loop operation, even when the plant is unstable. Experience with these methods has suggested, however, that the covariance of the estimates can be large for standard choices of instruments. Therefore, we have combined the TR and NF methods with the RIV-AML method to obtain more accurate estimates. If the open-loop plant is stable, this presents no problem: the hybrid techniques, termed TR/RIV-AML and NF/RIV-AML, can be synthesized without additional modifications. However, if the open-loop plant is unstable, many of the prefilters required by the RIV-AML procedure (Eqs. (22) and (24)) are also unstable—they contain $1/A(z)$, which is unstable if implemented as a causal filter.

To use the TR/RIV-AML and NF/RIV-AML procedure when the open-loop plant is unstable, we must modify the prefiltering scheme to avoid filters which are unstable. This problem is primarily one of understanding the prefilters in the context of the maximum-likelihood (ML) problem, and applying them properly. To develop the RIV-AML method, Young (1984) first writes the log-likelihood function for the observations $y(k)$, and then reduces the ML problem to the minimization of the following term:

$$L = \left[\frac{D}{C}\left(y - \frac{B}{A} \cdot u \right) \right]^T \left[\frac{D}{C}\left(y - \frac{B}{A} \cdot u \right) \right].$$

The RIV and AML prefilters are then formulated by writing $\partial L/\partial a_i = 0$, $\partial L/\partial b_i = 0$, etc. Thus the prefilters contain $1/\hat{A}$ because the log-likelihood function contains the prediction error

$$\left(y - \frac{\hat{B}}{\hat{A}} \cdot u \right).$$

When the closed-loop system is stabilizing an open-loop unstable plant, we are faced with the following prolblem: $y(k)$ and $u(k)$ are "stable" signals: that is, their Z-transforms $y(z)$ and $u(z)$ converge on the unit circle ($|z| = 1$). But $B(z)/A(z)$ is unstable; that is, it is the Z-transform of a causal impulse

response, and it contains poles outside the unit circle. Given these conditions, can we compute an estimate of $y(k)$ based on $u(k)$, $A(z)$, and $B(z)$ alone? If we can, then the prediction error can be formulated, and the prefilters necessary for the RIV-AML procedure can be found.

To answer this question, consider our system representation (13, 21):

$$y(z)=\frac{B(z)}{A(z)}\cdot u(z)+\frac{C(z)}{D(z)}\cdot\xi(z). \tag{31}$$

We can break $A(z)$ into a polynomial whose roots are stable, times a polynomial whose roots are unstable:

$$A(z)\equiv A_s(z)\cdot A_u(z), \tag{32}$$

where:

$$A_s(z)=\prod_j (1-v_j\cdot z^{-1});\ |v_j|<1,$$

$$A_u(z)=\prod_j (1-p_i\cdot z^{-1});\ |p_i|\geq 1.$$

This factorization of $A(z)$ allows us to rewrite (31) to reflect the possibility that the noise dynamics are affected by the unstable poles:

$$y(z)=\frac{B(z)}{A_u(z)A_s(z)}\cdot u(z)+\frac{E(z)}{A_u(z)F(z)}\cdot\xi(z). \tag{33}$$

where E/F is defined such that $C/D=E/A_uF$. Generality is retained in this formulation because $E(z)$ cancels any poles of $A_u(z)$ that are not part of $D(z)$. The transfer function E/F is stable if the system is stabilizable, so we can write:

$$\begin{aligned} y(z)&=\frac{1}{A_u(z)}\cdot\left[\frac{B(z)}{A_s(z)}\cdot u(z)+\frac{E(z)}{F(z)}\cdot\xi(z)\right]\\ &\equiv\frac{1}{A_u(z)}\cdot[q(z)] \end{aligned} \tag{34}$$

where $q(z)$ is bounded for $|z|=1$, because of the our conditions on A_s (stated in (32)), E/F (stated above), $u(k)$ (its Z-transform converges on the unit circle), and $\xi(k)$ (stated after (21)—the important point being that $\xi(k)$ is a finite-duration (windowed) sequence). We have also specified that a feedback system is stabilizing the plant, so that $y(z)$ converges for $|z|=1$. Thus, by studying (34), one concludes that $q(z)$ *must* contain zeros which cancel the unstable poles of $1/A_u$. We write this condition as follows:

$$\begin{aligned} q(z)&=A_u(z)\cdot w(z)\\ \Rightarrow y(z)&=\frac{1}{A_u(z)}\cdot[A_u(z)\cdot w(z)]. \end{aligned} \tag{35}$$

where $w(z)$ also converges for $|z|=1$. The pole-zero cancellation implied by (35) can be derived constructively (although somewhat tediously) by writing the closed-loop transfer function from *any* external signal (such as $r(z)$ or $\xi(z)$) to $y(z)$.

The representation (35) can be used to motivate a filtering scheme as follows: $1/A_u(z)$ is the (two-sided) Z-transform of at least *two distinct impulse responses* (Oppenheim and Schafer, 1989): 1) a causal, unstable impulse response, which we will call h_c, and 2) an anticausal, stable impulse response, which we will call h_{ac}. The Z-transform of h_c converges in the region of convergence (ROC) $|z|\geq\max(p_i)$, while the Z-transform of h_{ac} converges in the ROC $|z|<\min(p_i)$ (see Fig. 5). The ambiguity of the Z-transform is usually cleared up by invoking causality: because (31) represents a causal dynamic system, we known that the physically meaningful inverse of $1/A_u(z)$ is $h_c(k)$, and that the convolution corresponding to (35) is:

$$y(k)=h_c(k)*[h_A(k)*w(k)], \tag{36}$$

where $*$ indicates convolution and

$$\begin{aligned} h_c(k)&\equiv Z^{-1}\left\{\frac{1}{A_u(z)}\right\} &&\text{ROC: } |z|>\max(p_i),\\ h_A(k)&\equiv Z^{-1}\{A_u\} &&\text{ROC: all } z. \end{aligned}$$

As we have noted, $h_c(k)$ is causal, but because the poles of $1/A_u(z)$ lie outside the unit circle, $h_c(k)$ grows without bound as $k\to\infty$. However, it can be shown that the causal, unstable impulse response $h_c(k)$ can be replaced by its anticausal, stable counterpart $h_{ac}(k)$, *if* a pole-zero cancellation such as (35) occurs. We can write this statement as follows:

$$h_{ac}(k)*[h_A(k)*w(k)]=h_c(k)*[h_A(k)*w(k)] \tag{37}$$

where

$$h_{ac}(k)=Z^{-1}\left\{\frac{1}{A_u(z)}\right\}\quad\text{ROC: } |z|<\min(p_i).$$

Note here that the ROC overlaps the unit circle. Computing the inverse Z-transform over this ROC results in an impulse response which is bounded for all k (Oppenheim and Schafer, 1989). Thus we expect that replacing h_c with h_{ac} will yield a stable (although noncausal) way to predict $y(k)$.

Substituting (37) into (36), we have the following equation for $y(k)$:

$$y(k)=h_{ac}(k)^*[h_A(k)^*w(k)]. \tag{38}$$

Since all of the sequences in this equation are stable, their Z-transforms exist on the unit circle, and we can convert back to the Z-domain:

$$\begin{aligned} y(z)&=\left.\frac{1}{A_u(z)}\right|_{\text{ac}}\cdot[A_u(z)\cdot w(z)]\\ &=\left.\frac{B(z)}{A(z)}\right|_{\text{snc}}\cdot u(z)+\left.\frac{C(z)}{D(z)}\right|_{\text{snc}}\xi(z).\\ \Rightarrow\hat{y}(z)&=\left.\frac{\hat{B}(z)}{\hat{A}(z)}\right|_{\text{snc}}\cdot u(z), \end{aligned} \tag{39}$$

where we denote the Z-transform of h_{ac} as $1/A_u(z)|_{\text{ac}}$, to distinguish it from the Z-transform of h_c. The operations between transfer functions implied by (39) are valid for the transfer functions and signals we have defined, because they all converge on the unit circle. The subscript "snc" is used to indicate that we will use a stable, noncausal time-domain implementation of the filter—the anticausal part coming from the unstable poles, and the causal part coming from the stable poles. Figure 5 is an example of the regions of convergence associated with $1/A(z)$, and the corresponding impulse responses.

We have shown how the transfer function between $u(z)$ and $\hat{y}(z)$ must be altered when the open-loop plant is unstable. It can be shown that all of the filtering and prediction described in Section 2.2 can be similarly altered, without changing the maximum-likelihood results of Young (1984). Thus, our scheme is noncausal when the plant is unstable, and must be implemented off-line, but otherwise it proceeds as described in Sections 2.1–2.3, with $1/A(z)$ replaced by $1/A(z)|_{\text{snc}}$.

2.5 Application to the MIMO Rotating Stall System. The rotating stall system described in Eq. (11) is both multi-modal and MIMO. The multi-modal nature of the system requires dynamics to be identified for each mode number n. This identification can be done mode-by-mode, since the dynamics are decoupled. Equation (11) also shows that each mode constitutes a two-input two-output system. This adds complexity, but otherwise requires no modification to the procedure. Some specifics of the rotating stall analysis will be given, as an illustration and to demonstrate an algorithmic simplification.

The one-step ahead predictor for the system described in Eq. (11) is:

$$\begin{bmatrix} \hat{y}_{1_n} \\ \hat{y}_{2_n} \end{bmatrix}_k = \Phi_n^T(k) \cdot \hat{\Theta}_n$$

where: (40)

$$\Phi_n^T(k) = \begin{bmatrix} \Phi_{1_n}^T \\ \Phi_{2_n}^T \end{bmatrix}_k$$

$$= \begin{bmatrix} -y_1(k-1) & -y_1(k-2) & u_1(k)+u_1(k-1) & u_1(k-1)+u_1(k-2) & -u_2(k) & -u_2(k-1) & -u_2(k-2) \\ -y_2(k-2) & -y_2(k-2) & u_2(k)+u_2(k-1) & u_2(k-1)+u_2(k-2) & u_1(k) & u_1(k-1) & u_1(k-2) \end{bmatrix}_n$$

$$\hat{\Theta}_n = [a_1\ a_2\ b_1\ b_2\ b_3\ b_4\ b_5]_n^T$$

The instruments must match the dimension of the measurement matrix:

$$\zeta_n(k) = \begin{bmatrix} \zeta_{1_n}^T \\ \zeta_{2_n}^T \end{bmatrix} = \begin{bmatrix} \zeta_{11}(k) & \zeta_{21}(k) & \cdots & \zeta_{71}(k) \\ \zeta_{12}(k) & \zeta_{22}(k) & \cdots & \zeta_{72}(k) \end{bmatrix}_n^T. \quad (41)$$

Equations (17) through (28) proceed as before, with the understanding that the summations now contain matrix multiplications rather than scalar and inner products. Equation (19) can be made more efficient computationally by breaking up the matrices $\zeta_n(k)$ and $\Phi_n(k)$ into their constituent vectors. The resulting solution to the IV problem is as follows:

$$\hat{\Theta}_n = [\Sigma\zeta_{1_n} \cdot \Phi_{1_n}^T + \Sigma\zeta_{2_n} \cdot \Phi_{2_n}^T]^{-1} \cdot [\Sigma\zeta_{1_n} \cdot x_{1_n} + \Sigma\zeta_{2_n} \cdot x_{2_n}], \quad (42)$$

where subscripts k have been suppressed.

3 Results and Discussion

The techniques above were used on data collected from the active control research compressor. The pressure rise-flow coefficient characteristic for this compressor is shown in Fig. 6. Points below $\bar{\phi} \cong 0.45$ are unstable, so these data points are taken with the system operating in closed loop. Data points in the stable regime can also be taken in closed loop. This has been done and the pressure rise of the compressor is essentially unaffected by the controller.

A typical closed-loop IV parameter identification experiment is conducted as follows: First, the control system is initialized and closed-loop operation begins. Next, the downstream throttle is used to manually set the flow coefficient to the value at which the test will be run. This may or may not be an open-loop unstable operating point. The external signal $[r_1(k)\ r_2(k)]_n^T$ is then applied, and measurements are made of $[u_1(k)\ u_2(k)]_n^T$ and $[y_1(k)\ y_2(k)]_n^T$. The test can then be repeated for the TR method. The complete data set is then put through the TR/RIV-AML procedure or the NF/RIV-AML procedure described in Section 2. Estimates of A, B, C, and D are needed to initialize these algorithms. Typically the procedure is to use estimates of A, B, C, and D from a more stable $\bar{\phi}$ as initial guess for a less stable $\bar{\phi}$.

Numerical results appear in Tables 1 and 2 for operating points between $\bar{\phi} = 0.40$ and $\bar{\phi} = 0.55$, for $n = 1$ and 2. Also shown for comparison in these tables are parameter estimates obtained using the spectral estimation techniques described by Paduano (1992) (during open-loop operation above $\bar{\phi} = 0.45$).

A portion of a typical data set appears in Fig. 7, taken at $\bar{\phi} = 0.40$ for a mode number of one ($n = 1$). The command is a band-limited pseudo-random binary signal of magnitude 10° on each channel of the input vector $[r_1\ r_2]_n^T$. The bandwidth of the input is limited to $\omega = 1.1$ (50 Hz), which is about five times the natural frequency (ω_{rs_1}) of the system. The actual IGV deflections, $[u_1\ u_2]_n^T$, are responding to both this command and the feedback signal, as shown in Fig. 4 and in Eq. (29). It is apparent from the differences between $[r_1\ r_2]_{n=1}^T$ and $[u_1\ u_2]_{n=1}^T$ that the feedback signal is a major part of the excitation to the system. The outputs $[y_1\ y_2]_{n=1}^T$ are also shown in Fig. 7.

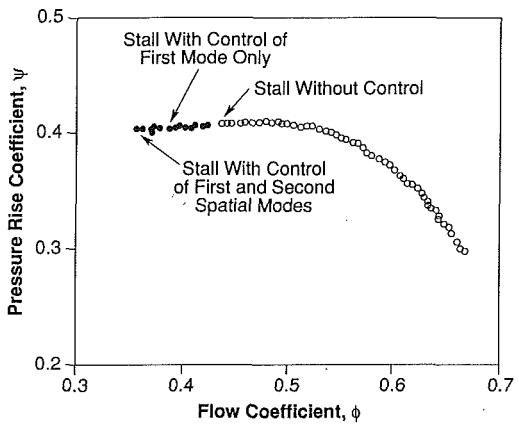

Fig. 6 Pressure rise characteristics for the active control research compressor

Table 1 Parameter estimates, $n = 1$

Spectral estimates (from (Paduano, 1992))					
$\bar{\phi}$	σ	ω_{rs}	b_r	b_i	g_i
0.475	−6.27	67.29	−4.81	2.03	−0.055
0.500	−15.58	71.71	−5.55	2.18	−0.061
0.525	−26.50	65.98	−5.70	1.05	−0.059
0.550	−36.37	50.81	−5.57	−0.84	−0.059
NF/RIV-AML estimates					
$\bar{\phi}$	σ	ω_{rs}	b_r	b_i	g_i
0.400	5.50	52.27	−3.00	1.01	−0.029
0.425	0.61	56.99	−3.10	1.36	−0.033
0.450	−1.62	63.54	−3.56	1.49	−0.039
0.475	−4.96	66.42	−3.91	2.14	−0.044
0.500	−13.50	67.20	−4.75	2.14	−0.050
0.525	−26.27	60.36	−4.90	1.17	−0.051
TR/RIV-AML estimates					
$\bar{\phi}$	σ	ω_{rs}	b_r	b_i	g_i
0.400	4.95	55.15	−3.19	0.90	−0.036
0.425	1.26	59.86	−2.80	0.80	−0.035
0.450	−1.79	63.32	−3.69	1.50	−0.038
0.475	−4.88	68.53	−3.97	2.03	−0.044

Table 2 Parameter estimates, $n = 2$

Spectral estimates (from (Paduano, 1992))					
$\bar{\phi}$	σ	ω_{rs}	b_r	b_i	g_i
0.475	−32.46	157.37	−11.57	−0.54	−0.048
0.500	−52.38	168.26	−12.68	−1.28	−0.050
0.525	−77.44	188.59	−15.93	−2.16	−0.060
0.550	−93.17	181.28	−16.36	−3.76	−0.065
NF/RIV-AML estimates					
$\bar{\phi}$	σ	ω_{rs}	b_r	b_i	g_i
0.400	−4.40	137.44	−8.07	0.91	−0.038
0.425	−13.42	144.45	−9.12	0.62	−0.042
0.450	−27.63	152.40	−10.27	0.13	−0.044
0.475	−36.97	157.67	−11.24	0.01	−0.047
0.500	−49.78	159.42	−11.36	−0.22	−0.044
0.525	−75.22	152.07	−11.34	−2.16	−0.041
TR/RIV-AML estimates					
$\bar{\phi}$	σ	ω_{rs}	b_r	b_i	g_i
0.375	0.91	123.16	−7.28	0.63	−0.057
0.400	−3.42	137.27	−7.90	1.01	−0.039
0.425	−13.31	144.14	−8.91	0.60	−0.041
0.450	−24.81	151.65	−9.94	0.17	−0.043
0.475	−37.48	158.56	−11.27	−0.25	−0.047

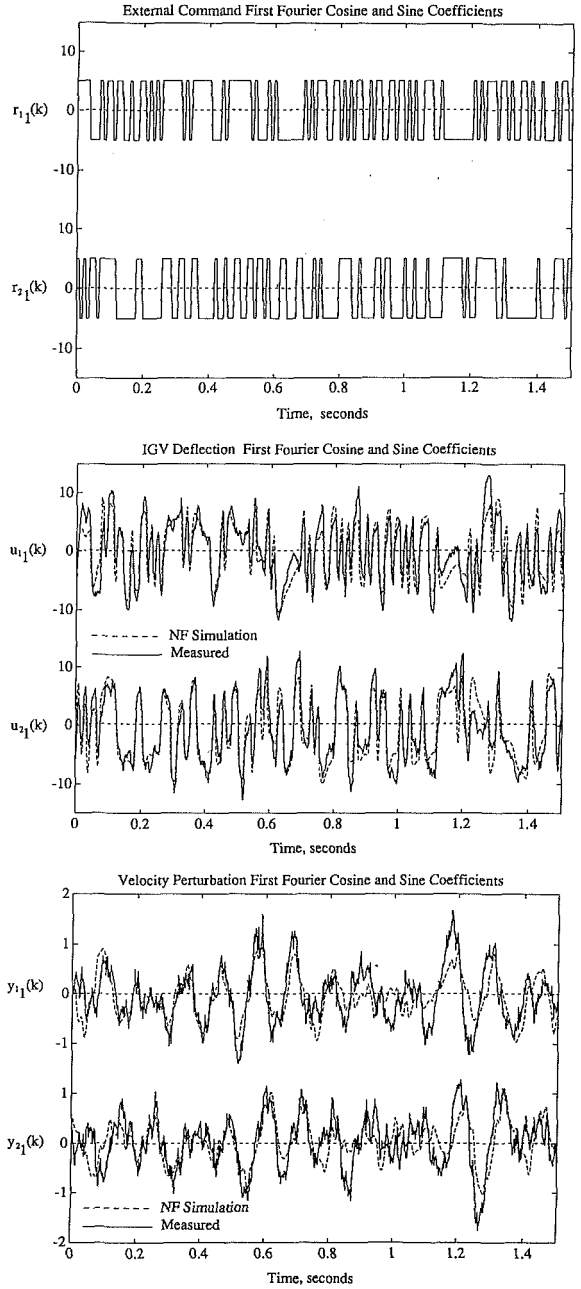

Fig. 7 Results of a typical identification run. Solid lines are experimental data, dashed lines are predictions based on the parameter estimates (noise-free simulation) $\phi = 0.40$.

An important step in a parameter identification procedure is model and parameter validation. Here we present several results which indicate that the system structure and identified parameters do in fact model the system well. The first is shown in Fig. 7, where a simulation based on the parameter estimates is used to predict the values of u_k and y_k. This is *not* the output of a one-step ahead predictor, which would rely on past measurements to make the prediction. Rather, it is a simulation based solely on r_k, the identified parameters of $\bar{\phi} = 0.40$, and the controller and sensor dynamics. The fit is quite good, even though the simulation is noise-free, while the experiment is not: u_k and y_k in the experiment are responding to excitation noise in the compressor. Fits of this quality can be gotten regardless of whether the data to be fit is used to get the estimates. Since the noise free simulation results are used as the instruments in the NF/RIV-AML method, Fig. 7 also serves to validate that a high degree of correlation in fact exists between the instruments and the measurements.

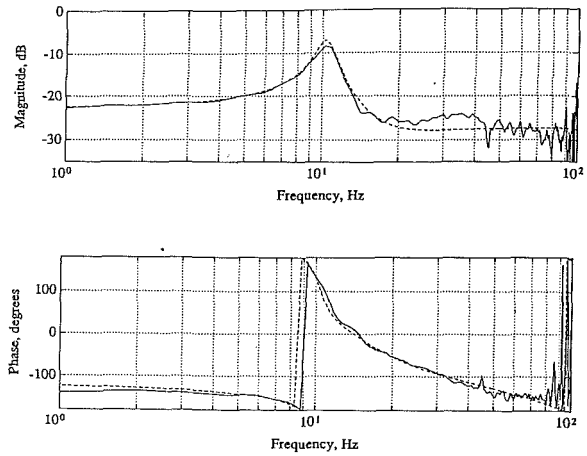

Fig. 8 Comparison of spectral estimation results (Paduano, 1992) and IV parameter identification results. Solid line is an empirical transfer function estimate, dashed line is a transfer function derived from parameters which were identified during closed-loop operation. $\phi = 0.475$.

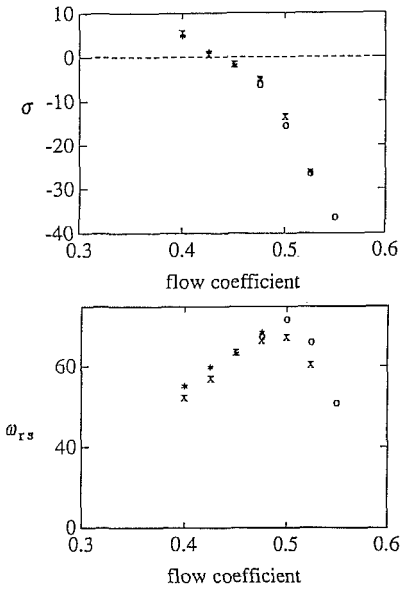

Fig. 9 Parameter variations with flow coefficient. o -Open-loop parameter estimates (from (Paduano, 1992)); * -TR/RIV-AML results; x -NF/RIV-AML results.

The closed-loop IV methods (TR/RIV-AML and NF/RIV-AML) are designed to operate in a regime where the spectral estimation procedure presented by Paduano (1992) gives poor results, that is, during stabilization of unstable operating points. However, closed-loop data sets can be taken at flow coefficients which are open-loop stable. Such tests can be used to verify that closed-loop IV methods properly account for the loop closure and still provide good estimates. Figure 8 shows the results of such a test. A spectral estimate (based on open-loop data, using the techniques in Paduano (1992)) is compared to both a TR/RIV-AML and NF/RIV-AML estimate (based on closed-loop data). Good agreement between the frequency responses is obtained. This agreement is important, because IV-based estimates of $G_n(s)$ not only use the estimated parameters, but also assume a certain model structure. Since spectral estimates are parameter-free and assume no specific model structure, this comparison verifies both the parameter estimates and the model structure.

Finally, the estimates of the parameters from various methods can be compared graphically, to see if the trends with $\bar{\phi}$ are smooth. Figure 9 shows σ_1 and ω_{rs_1} as a function of flow

coefficient, plotting spectral, TR/RIV-AML, and NF/RIV-AML results on the same plot. Within reasonable error bands, all of the estimation methods yield the same curves.

The data presented here are a small sample of the data taken, and are intended only to demonstrate the practical applicability of the identification methods. A complete presentation of the data, together with detailed discussion of the physical significance of the parameter estimates, appears in Paduano (1992), and requires a more complete description of rotating stall modeling. For this discussion, the relevant conclusion of the experiments is that the methods presented here yield consistent, accurate results, with good convergence properties and little sensitivity to the stability of the plant. Established prediction error methods, such as those provided in (Ljung, 1987), have similar properties (for the data sets tested). These methods utilize nonlinear search schemes to minimize prediction error, instead of the least-squares type approach utilized by IV methods. Only a thorough comparison of these two approaches would allow one to judge their relative merits. Wellstead (1981) also discusses a scheme for *non-parametric* estimation of forward-path transfer functions during closed-loop operation. This method would allow one to deduce the desired plant dynamics (using transfer-function fits to the nonparametric estimates (Paduano, 1992)), if sufficient care were taken to model other contributions to the forward-path transfer function. Again, the relative merits of Wellstead's method and the method presented here can only be determined by a thorough comparison.

4 Conclusions

By combining various extensions to the basic instrumental variable approach, a scheme for estimating parameters in an unstable system operating closed loop has been developed. This scheme was successfully applied to a model for the distributed dynamics of an experimental axial compressor. Thus the usefulness of the procedure and the validity of the model were both verified experimentally.

Acknowledgments

The authors would like to thank Dr. Jon Simon and Professor Lennart Ljung for critically reviewing this work. This work was supported by U.S. Air Force Office of Scientific Research, Dr. J. M. McMichael, Technical Monitor, and by the Office of Naval Research, Dr. R. J. Hansen, Technical Monitor. This support is gratefully acknowledged.

References

Åström, K. J., and Wittenmark, B., 1984, *Computer Controlled Systems—Theory and Design*, Prentice-Hall, New Jersey.

Epstein, A. H., Ffowcs-Williams, J. E., and Greitzer, E. M., 1989, "Active Suppression of Aerodynamic Instabilities in Turbomachines," *J. Propulsion*, Vol. 5, No. 2, pp. 204–211.

Greitzer, E. M., 1976, "Surge and Rotating Stall in Axial Flow Compressors; Part I: Theoretical Compression System Model," ASME *Journal of Engineering for Power*, Vol. 98, pp. 190–198.

Greitzer, E. M., 1980, "Review—Axial Compressor Stall Phenomena," ASME *Journal of Fluids Engineering*, Vol. 102, pp. 134–151.

Hynes, T. P., and Greitzer, E. M., 1987, "A Method for Assessing Effects of Inlet Flow Distortion on Compressor Stability," ASME *Journal of Turbomachinery*, Vol. 109, pp. 371–379.

Kerrebrock, J. L., 1977, *Aircraft Engines and Gas Turbines*, The MIT Press, Cambridge, MA, pp. 154–155.

Ljung, L., 1987, *System Identification—Theory for the User*, Prentice-Hall, New Jersey.

Moore, F. K., 1984, "A Theory of Rotating Stall of Multistage Compressors," ASME *Journal of Engineering for Power*, Vol. 106, p. 313.

Oppenheim, A. V., and Schafer, R. W., 1989, *Discrete-Time Signal Processing*, Prentice-Hall, New Jersey.

Paduano, J., Epstein, A. H., Valavani, L., Longley, J. P., Greitzer, E. M., and Guennette, G. R., 1991, "Active Control of Rotating Stall in a Low Speed Axial Compressor," ASME Paper 91-GT-88, Proceedings, ASME International Gas Turbine Conference, Orlando. To be published in ASME JOURNAL OF DYNAMIC SYSTEMS, MEASUREMENT, AND CONTROL.

Paduano, J. D., 1992, "Active Control of Rotating Stall in Axial Compressors," Ph.D. thesis, MIT Dept. of Aeronautics and Astronautics. Also available as MIT Gas Turbine Laboratory Report #208.

Söderström, T., Stoica, P., and Trulsson, E., 1987, "Instrumental Variable Methods for Closed Loop Systems," *Automatic Control—World Congress, 1987*, Selected Papers from the 10th Triennial World Congress of IFAC, Munich, July, pp. 363–368.

Wang, H., and Cao, D., 1989, "Two Instrumental Variable Methods for Closed Loop System Identification," *Identification and System Parameter Estimation 1988*, Selected Papers from the Eighth IFAC/IFORS Symposium, Beijing, Aug., p. 543.

Wellstead, P. E., 1981, "Non-Parametric Methods of System Identification," *Automatica*, Vol. 17, No. 1, pp. 55–69.

Young, P., 1984, *Recursive Estimation and Time-Series Analysis*, Springer-Verlag.